

# SINGLE PRODUCTION OF SLEPTONS WITH POLARIZED TOPS AT THE LARGE HADRON COLLIDER

Masato Arai<sup>(1)†</sup>, Katri Huitu<sup>(2)‡</sup>, Santosh Kumar Rai<sup>(2,3)\*</sup>  
and Kumar Rao<sup>(2)\*\*</sup>

<sup>(1)</sup> *Institute of Experimental and Applied Physics, Czech Technical University in Prague,  
Horská 3a/22, 128 00 Prague 2, Czech Republic*

<sup>(2)</sup> *Department of Physics, University of Helsinki, and Helsinki Institute of Physics,  
P.O. Box 64, FIN-00014 University of Helsinki, Finland*

<sup>(3)</sup> *Department of Physics, and Oklahoma Center for High Energy Physics,  
Oklahoma State University Stillwater, OK 74078, USA*  $\diamond$

## Abstract

We study the production of a single charged slepton in association with a top quark in a R-parity violating supersymmetric model with lepton number violating interactions at the Large Hadron Collider. We find that the longitudinal polarization asymmetry of the top quark in such a production mode is significantly different from that in the production of a single top or a top pair in the Standard Model for a wide range of slepton masses. Our signal analysis shows that the top-slepton associate production leads to final states with distinct kinematic signatures, which differ from the Standard Model background.

PACS: 12.60.Jv, 13.88.+e, 14.80.Ha, 14.80.Ly

<sup>†</sup>masato.arai@utef.cvut.cz

<sup>‡</sup>katri.huitu@helsinki.fi

\*santosh.rao@okstate.edu ( $\diamond$  current address)

\*\*kumar.rao@helsinki.fi

# 1 Introduction

The most promising candidate theory beyond the Standard Model (SM) remains supersymmetry (SUSY), which resolves some of the shortcomings of the SM such as the gauge hierarchy problem. In many supersymmetric models, a discrete multiplicative symmetry [1], R-parity, defined by  $R_p = (-1)^{3B+L+2S}$  with spin  $S$ , baryon number  $B$ , and lepton number  $L$ , is often imposed on the Lagrangian to conserve  $B$  and  $L$ . The definition implies that all the SM particles have  $R_p = +1$ , while all the superpartners are odd under this symmetry. This conservation is, however, not dictated by any fundamental principle such as gauge invariance or renormalizability.

The most general superpotential in SUSY, which respects the gauge symmetries of the SM, contains bilinear and trilinear terms, which do not conserve either  $B$  or  $L$  and are given by

$$\mathcal{W}_{R_p} = \frac{1}{2}\lambda_{ijk}\hat{L}_i\hat{L}_j\hat{E}_k + \lambda'_{ijk}\hat{L}_i\hat{Q}_j\hat{D}_k + \frac{1}{2}\lambda''_{ijk}\hat{U}_i\hat{D}_j\hat{D}_k + \mu_i\hat{L}_i\hat{H}_2, \quad (1)$$

where  $\hat{L}_i, \hat{Q}_i$  are the  $SU(2)$ -doublet and  $\hat{E}_i, \hat{U}_i, \hat{D}_i$  are the  $SU(2)$ -singlet superfields, respectively.  $\hat{H}_2$  is the Higgs chiral superfield. The indices,  $i, j, k$  denote generations. The  $\lambda, \lambda'$  and  $\mu$  are the couplings of the  $L$ -violating interactions, whereas  $\lambda''$  are those of the  $B$ -violating interactions. The co-existence of the  $L$ - and  $B$ - violating interactions leads to phenomenological difficulties unless R-parity violating (RPV) couplings are very small: the simultaneous presence of both  $L$ - and  $B$ -violating operators could lead to a very rapid proton decay, especially for TeV scale sparticle masses. Thus, the products of the  $L$ - and  $B$ -violating couplings are strictly constrained [2]. In phenomenological studies usually only one type of interaction, either  $L$ - or  $B$ -violating, is considered. This can be realized, for instance, by imposing a discrete ( $Z_3$ ) symmetry [3]. The RPV couplings can also lead to small neutrino masses, which are automatically generated either at tree- or loop-level [4]. For a comprehensive review of RPV interactions, see [5]. Constraints on the RPV couplings have been obtained by various analysis, for review see [5, 6].

RPV interactions can lead to new production mechanisms for single top quarks. Associate production of single top quarks in SUSY models with RPV interactions have been extensively studied for several processes, see e.g. [7, 8]. In these processes, top quarks are produced via  $L$ - or  $B$ -violating Yukawa type couplings given in Eq. (1). An important property of the top, in contrast to lighter quarks, is that its spin is observable since it decays before hadronization,

owing to its extremely short lifetime. In the SM single top quarks are produced through the parity violating weak interactions, leading to highly polarized top quarks [9, 10]. The polarizations of the top quarks produced through RPV interactions and the SM would be different, since different chiral structures are involved in the interaction vertices. Effects of RPV interactions on polarized single top production and CP odd observables associated with top quark spin have been studied at a leptonic collider [11]. Polarization of top quark produced in the process  $d\bar{d} \rightarrow t\bar{t}$  through RPV interaction has been addressed at the Tevatron [12] and the Large Hadron Collider (LHC) [13]. Even in parity conserving QCD, though the top is produced unpolarized, the spin of the top is correlated with that of the antitop for top pair production processes. Searches for new physics by using top spin correlations (e.g. see [14] and references therein) and single top polarization [15] have been studied.

In this work, we study single charged slepton production in association with a top quark at the LHC through the interaction  $\lambda'_{i3k} L_i Q_3 \bar{D}_k$  in Eq. (1), which violate lepton number by one unit. Written in terms of the component fields, the relevant terms for the above superpotential lead to the interaction Lagrangian

$$\begin{aligned} \mathcal{L}_{LQ\bar{D}} = & \lambda'_{i3k} \left[ \tilde{\nu}_{iL} \bar{d}_{kR} d_{3L} + \tilde{d}_{3L} \bar{d}_{kR} \nu_{iL} + (\tilde{d}_{kR})^* \overline{(\nu_{iL})^c} d_{3L} \right. \\ & \left. - \tilde{\ell}_{iL} \bar{d}_{kR} u_{3L} - \tilde{u}_{3L} \bar{d}_{kR} \ell_{iL} - (\tilde{d}_{kR})^* \overline{(\ell_{iL})^c} u_{3L} \right] + \text{h.c.} \end{aligned} \quad (2)$$

where the superscript “ $c$ ” in the above equation represents the charge conjugation of the spinor ( $\psi^c = C\bar{\psi}^T$ ),  $C$  being the charge conjugation operator. For example  $(\nu_{iL})^c \equiv (\nu^c)_{iR}$ . These interactions lead to the production process  $gd_k \rightarrow t\tilde{\ell}_i$ , which we investigate in this work. The same process has been considered in [7], but the polarization of the top quark has not been investigated there. In this work, we investigate the effects of RPV couplings on the polarization asymmetry of the top quark, which is the (normalized) difference between the number of produced tops with spin up and spin down. We also show, how the properties of a polarized top are reflected in the decay products by performing a detailed signal analysis. We focus on leptonic decays of the top, which will have the cleanest signals at the LHC. We also highlight special kinematic variables, which are sensitive to polarization effects and can lead to hints about the nature of the new physics that plays a role in the production of a single top.

In Section 2 we discuss the top polarization and give the basic framework of our calculations using the spin density matrix. In Section 3 we present helicity amplitudes and

the polarized cross sections for the process that we study at LHC. In Section 4 we show results for the signal and SM background analysis and present the LHC reach for the signal in Section 5. We summarize in Section 6.

## 2 Top polarization and the spin density matrix

With a large mass of  $\sim 173$  GeV [16], the top quark has an extremely short lifetime, calculated in the SM to be  $\tau_t = 1/\Gamma_t \sim 5 \times 10^{-25}$  s. This is an order of magnitude smaller than the hadronization time scale, which is roughly  $1/\Lambda_{\text{QCD}} \sim 3 \times 10^{-24}$  s. Thus the top decays before it can form bound states with lighter quarks [17]. As a result, the spin information of the top, which depends on its production process, is reflected in characteristic angular distributions of its decay products. Even if the top were to form hadrons, the spin flip time scale induced by QCD spin-spin interactions between the top and light anti-quark, is of the order of  $m_t/\Lambda_{\text{QCD}}^2$ , which is much larger than  $\tau_t$ . Thus the degree of polarization of an ensemble of top quarks can provide important information about the underlying physics in its production, apart from usual variables like cross sections. For a review on top quark physics and polarization see [18, 19, 20].

Top spin can be determined by the angular distribution of its decay products. In the SM, the dominant decay mode is  $t \rightarrow bW^+$ , with a branching ratio (BR) of 0.998, with the  $W^+$  subsequently decaying to  $\ell^+\nu_\ell$  (semileptonic decay) or  $u\bar{d}$ ,  $c\bar{s}$  (hadronic decay). The angular distribution of a fermion  $f$  for a top quark ensemble in the top rest frame has the form [21]

$$\frac{1}{\Gamma_f} \frac{d\Gamma_f}{d\cos\theta_f} = \frac{1}{2}(1 + \kappa_f P_t \cos\theta_f), \quad (3)$$

where  $\Gamma_f$  is the partial decay width,  $\theta_f$  is the angle between the direction of the motion of decay fermion  $f$  and the top spin vector, in the top rest frame and

$$P_t = \frac{N_\uparrow - N_\downarrow}{N_\uparrow + N_\downarrow} \quad (4)$$

is the degree of polarization of the top quark ensemble, where  $N_\uparrow$  and  $N_\downarrow$  refer to the number of positive and negative helicity tops, respectively. The coefficient  $\kappa_f$  is called the spin analyzing power of  $f$  and it is a constant between  $-1$  and  $1$ . Obviously, a larger  $\kappa_f$  makes  $f$  a more sensitive probe of the top spin. At tree-level, the charged lepton and  $d$  quark are the best spin analyzers with  $\kappa_{\ell^+} = \kappa_{\bar{d}} = 1$ , while  $\kappa_{\nu_\ell} = \kappa_u = -0.30$  and  $\kappa_b = -\kappa_{W^+} = -0.39$

[21, 22, 23, 24]. Thus the  $\ell^+$  or  $d$  have the largest probability of being emitted in the direction of the top spin and the least probability in the direction opposite to the spin. As mentioned in the introduction, at the LHC leptons can be measured with high precision. Therefore, in this paper we focus on leptonic decays of the top quark.

Let us consider a generic process of top production and its subsequent semileptonic decay  $AB \rightarrow tX \rightarrow b\ell^+\nu_\ell X$ , where  $X = P_1 P_2 \cdots P_{n-1}$  and  $P_i (i = 1, \cdots, n-1)$  are the other produced particles. Since  $\Gamma_t/m_t \sim 0.008$ , we can use the narrow width approximation to write the cross section as a product of the  $2 \rightarrow n$  production cross section times the decay width of the top. However, in probing top polarization using angular distributions of the decay lepton, it is necessary to keep the top spin information in production and decay, thus requiring the spin density matrix formalism. The amplitude for  $AB \rightarrow t(\lambda)X \rightarrow b\ell^+\nu_\ell X$  can be written as  $\sum_\lambda \mathcal{M}_P(\lambda) \mathcal{M}_D(\lambda)$  where  $\mathcal{M}_{P,D}(\lambda)$  are the amplitudes for the production and decay for an on-shell top with helicity  $\lambda = \pm 1$ . Thus, the amplitude squared is of the form

$$\begin{aligned} |\mathcal{M}(AB \rightarrow t(\lambda)X \rightarrow b\ell^+\nu_\ell X)|^2 &= \sum_{\lambda, \lambda'} \mathcal{M}_P(\lambda) \mathcal{M}_P^*(\lambda') \mathcal{M}_D(\lambda) \mathcal{M}_D^*(\lambda') \\ &\equiv \rho(\lambda, \lambda') \Gamma(\lambda, \lambda'), \end{aligned} \quad (5)$$

where  $\rho(\lambda, \lambda') = \mathcal{M}_P(\lambda) \mathcal{M}_P^*(\lambda')$  and  $\Gamma(\lambda, \lambda') = \mathcal{M}_D(\lambda) \mathcal{M}_D^*(\lambda')$  are the  $2 \times 2$  top production and decay spin density matrices. The off-diagonal elements encode the quantum mechanical interference between the production and decay amplitudes, which prevent a simple factorization of the process as a product of production and decay squared amplitudes,  $|\sum_\lambda \mathcal{M}_P(\lambda)|^2 |\sum_{\lambda'} \mathcal{M}_D(\lambda')|^2$ , where the spin information of the top is lost.

We consider the cross section of the  $2 \rightarrow n$  production. As in [15], the most general polarization density matrix can be parameterized as a linear combination of the Pauli matrices as

$$\sigma(\lambda, \lambda') = \frac{\sigma_{\text{tot}}}{2} \begin{pmatrix} 1 + \eta_3 & \eta_1 - i\eta_2 \\ \eta_1 + i\eta_2 & 1 - \eta_3 \end{pmatrix}, \quad (6)$$

where  $\sigma(\lambda, \lambda')$  is the cross section of  $2 \rightarrow n$  process of the top production at parton level with denoted spin labels and  $\sigma_{\text{tot}} = \sigma(+, +) + \sigma(-, -)$  is the total cross section. The (1,1) and (2,2) diagonal elements are the cross sections for the production of positive and negative

helicity tops and  $\eta_3$  gives the degree of *longitudinal* polarization

$$\eta_3 = P_t = \frac{\sigma(+, +) - \sigma(-, -)}{\sigma(+, +) + \sigma(-, -)}. \quad (7)$$

The off-diagonal elements involving  $\eta_1$  and  $\eta_2$  are the cross sections for transversely polarized tops. The degree of transverse polarization parallel and perpendicular to the production plane are given by

$$\eta_1 = \frac{\sigma(+, -) + \sigma(-, +)}{\sigma(+, +) + \sigma(-, -)}, \quad i\eta_2 = \frac{\sigma(+, -) - \sigma(-, +)}{\sigma(+, +) + \sigma(-, -)}. \quad (8)$$

By measuring the angular distributions of the decay lepton in the top rest frame (which requires reconstructing the top rest frame) analytic expressions for the  $\eta$ 's can be obtained by a suitable combination of lepton polar and azimuthal asymmetries (see [15] for details). However, at a hadron machine like the LHC, reconstruction of the top rest frame will be challenging leaving ambiguities in the measurement of such observables. Thus, the final state kinematics, as discussed later, will be of utmost importance in the top events.

### 3 Top-Slepton Production and Decay

#### 3.1 Density Matrix for Top-Slepton Production

In this subsection we derive a density matrix for the process of single top production in association with a charged slepton in R-parity violating SUSY. At the parton level the process is given by

$$g(p_1) d_k(p_2) \rightarrow t(p_3, \lambda_t) \tilde{\ell}_i^-(p_4), \quad (9)$$

which just employs the RPV part of the Lagrangian  $\left(\lambda'_{i3k}(\tilde{\ell}_{iL}\bar{d}_{kR}t_L)\right)$  given in Eq. (2). The relevant leading order diagrams are given in Fig. 1. Two diagrams contribute to the production process in Eq. (9) with the down-type quark ( $d_k$ ) in the  $s$ -channel and the top-quark in the  $t$ -channel as shown in Fig. 1 (a) and Fig. 1 (b), respectively.

The possible set of couplings one can probe with the process given by Eq. (9) is

$$\begin{aligned} \lambda'_{131}, \lambda'_{132}, \lambda'_{133} & \quad (\tilde{e} \text{ produced}), \\ \lambda'_{231}, \lambda'_{232}, \lambda'_{233} & \quad (\tilde{\mu} \text{ produced}), \\ \lambda'_{331}, \lambda'_{332}, \lambda'_{333} & \quad (\tilde{\tau} \text{ produced}). \end{aligned}$$

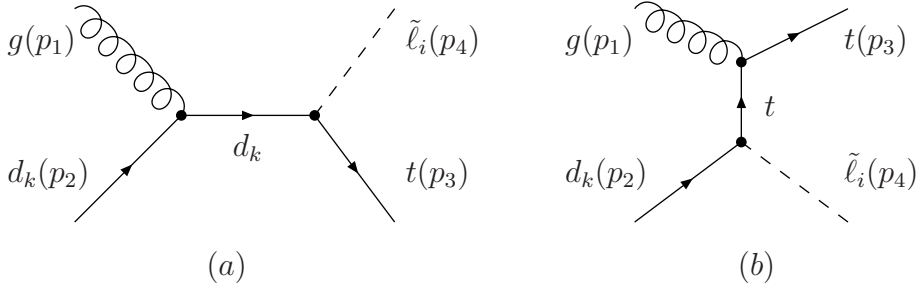


Figure 1: *The Feynman diagrams contributing to the top-slepton production at the parton level at LHC via RPV couplings.*

Some of the above couplings are strongly suppressed and so we can make a case out of each such coupling that is allowed in a range, which gives significant cross section at the LHC. For a summary of the various bounds on the above couplings see [5, 7].

As discussed in the previous section, to study the polarization properties of the top quarks produced at LHC we need to keep the spin information of the top as shown in Eq. (5). One can do that by writing down the helicity amplitudes for the process given by Eq. (9). The top polarization depends on the choice of spin quantization axis. Choices other than the helicity basis have been used in which the top is almost 100% polarized [10]. These are useful for low velocity tops produced near threshold and are relevant at the Tevatron. At the LHC, since we expect that the tops will be highly boosted, we choose the helicity basis. Denoting the helicity of the gluon, top and massless down-type quark  $d_k$  as  $h$ ,  $\lambda_t$  and  $\lambda_{d_k}$  respectively, the non-zero  $s$ -channel amplitudes are

$$\mathcal{M}_s(\lambda_t = +, \lambda_{d_k} = +) = -\sqrt{\frac{1}{2\sqrt{s}}} g_s \lambda'_{i3k} \left( \frac{\lambda_t}{2} \right) (1+h) \sqrt{E_t - p_t} \cos \frac{\theta}{2}, \quad (10)$$

$$\mathcal{M}_s(\lambda_t = -, \lambda_{d_k} = +) = \sqrt{\frac{1}{2\sqrt{s}}} g_s \lambda'_{i3k} \left( \frac{\lambda_t}{2} \right) (1+h) \sqrt{E_t + p_t} \sin \frac{\theta}{2}, \quad (11)$$

while the non-zero amplitudes for the  $t$ -channel are

$$\begin{aligned} \mathcal{M}_t(\lambda_t = +, \lambda_{d_k} = +) &= g_s \lambda'_{i3k} \left( \frac{\lambda_l}{2} \right) \sqrt{\frac{\sqrt{s}}{2}} \frac{1}{(t - m_t^2)} \left[ -m_t(1+h)\sqrt{E_t + p_t} \cos \frac{\theta}{2} \right. \\ &\quad \left. + (1+h)(E_t + p_t \cos \theta - \sqrt{s})\sqrt{E_t - p_t} \cos \frac{\theta}{2} - (1-h)p_t \sin \theta \sqrt{E_t - p_t} \sin \frac{\theta}{2} \right], \end{aligned} \quad (12)$$

$$\begin{aligned} \mathcal{M}_t(\lambda_t = -, \lambda_{d_k} = +) &= g_s \lambda'_{i3k} \left( \frac{\lambda_l}{2} \right) \sqrt{\frac{\sqrt{s}}{2}} \frac{1}{(t - m_t^2)} \left[ m_t(1+h)\sqrt{E_t - p_t} \sin \frac{\theta}{2} \right. \\ &\quad \left. - (1+h)(E_t + p_t \cos \theta - \sqrt{s})\sqrt{E_t + p_t} \sin \frac{\theta}{2} - (1-h)p_t \sin \theta \sqrt{E_t + p_t} \cos \frac{\theta}{2} \right], \end{aligned} \quad (13)$$

where  $s$  and  $t$  are the parton level Mandelstam variables and  $E_t$ ,  $p_t$  and  $\theta$  are the energy, momentum and scattering angle of the top in the parton center-of-mass frame and  $m_t$ ,  $\lambda_l$  are the top quark mass and  $SU(3)$  color matrices, while  $g_s$  is the QCD coupling constant.

Using these helicity amplitudes the elements of the top production spin density matrix can be constructed. We find the following compact expressions for  $\rho(\lambda, \lambda')$ :

$$\begin{aligned} \rho(+, +) &= \frac{F_1}{2} [A_1 + A_2 + A_3 \cos \theta], \\ \rho(-, -) &= \frac{F_1}{2} [A_1 - A_2 - A_3 \cos \theta], \\ \rho(+, -) &= \rho(-, +) \\ &= F_1 s \sqrt{s} m_t \sin \theta [-t^2 - st + tm_\ell^2 + tm_t^2 - sm_\ell^2 - m_t^2 m_\ell^2], \end{aligned} \quad (14)$$

with the various functions defined by

$$\begin{aligned} F_1 &= \frac{g_s^2 \lambda_{i3k}'^2}{24 s^2 (t - m_t^2)^2}, \\ A_1 &= -2s(s+t)^2(t - m_t^2) + 4stm_\ell^2(s+t - m_\ell^2) \\ &\quad + 2sm_t^2(m_t^4 + 2m_\ell^4 - 2sm_t^2 - tm_t^2 - 2m_t^2 m_\ell^2), \\ A_2 &= F_s [st(s+t) - sm_\ell^2(s+3t) + sm_t^2(2s+t - 2m_t^2 + 3m_\ell^2)], \\ A_3 &= s^2 t(s+t) + sm_\ell^2(s^2 - t^2 - 2st + tm_\ell^2 - sm_\ell^2) \\ &\quad + sm_t^2(t^2 + 2sm_\ell^2 - tm_t^2 + m_t^2 m_\ell^2 - m_\ell^4), \\ F_s &= \lambda^{1/2}(s, m_\ell^2, m_t^2), \\ \lambda(x, y, z) &= x^2 + y^2 + z^2 - 2xy - 2yz - 2xz. \end{aligned} \quad (15)$$

Here  $m_\ell$  is the slepton mass and the angular dependence in  $t$  is given by

$$t = m_t^2 - \frac{s + m_t^2 - m_\ell^2}{2} (1 - \beta_t \cos \theta),$$



where

$$\beta_t = \frac{F_s}{s + m_t^2 - m_\ell^2}.$$

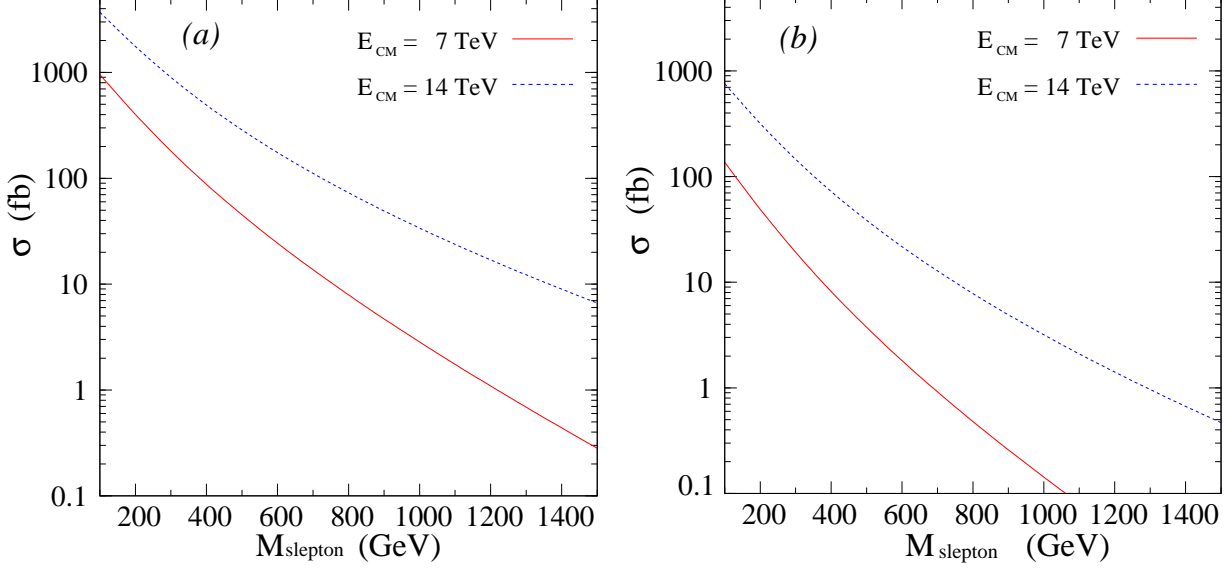


Figure 2: The cross section for top-slepton production at LHC for two different center-of-mass energies, 7 TeV and 14 TeV. (a) shows the cross section for top-slepton production via  $\lambda'_{i31}$  coupling and (b) shows the cross section for top-slepton production via  $\lambda'_{i32}$  coupling. We choose both  $\lambda' = 0.2$ .

A plot of the cross section for top-slepton production is shown in Fig. 2 as a function of the slepton mass, with  $d$  and  $s$  quarks in the initial state. Similar plots for the cross sections can also be found in [7]. The strong constraints on the  $\lambda'_{i33} < \mathcal{O}(10^{-4})$  [7] coupling indicate that there cannot be any significant production cross section at LHC for the process induced by  $b$  quarks in the initial state. To illustrate the cross sections, we have used a fixed value of 0.2 for the contributing RPV couplings, which in this case are  $\lambda'_{i31}$  and  $\lambda'_{i32}$  for  $d$  and  $s$  quarks, respectively. We show the cross sections for two different center-of-mass energies at which the LHC is now planned to run, viz. 7 TeV and 14 TeV. For the same strength of RPV coupling, the cross sections for the  $d$  quark induced process (Fig. 2 (a)) dominates the  $s$  quark induced process (Fig. 2 (b)) by nearly an order of magnitude, which is quite expected because of the large flux of  $d$  quarks compared to that of  $s$  quarks in the proton parton distribution. For our analysis, we have chosen the leading order parton density function (PDF) sets of CTEQ6L [25] for the colliding protons.

The  $(t d_k \tilde{\ell})$  vertex is proportional to the projection operator  $P_R = (1 + \gamma_5)/2$  and thus has a chiral structure different from the vector and axial vector interaction vertices for  $t\bar{b}W$  and  $t\bar{t}Z^0$ . The latter are relevant for  $tW$ ,  $t\bar{b}$  and  $t\bar{t}$  productions which are the dominant modes of top quark production at the LHC. We thus expect a different longitudinal polarization asymmetry given by Eq. (7) for top-slepton production, compared to the associated  $tW$  production via  $gb \rightarrow tW$  and the top pair production processes dominated by the  $gg$ ,  $q\bar{q} \rightarrow t\bar{t}$  or the  $W$  exchange process for  $t\bar{b}$  production in the SM. For  $tW$  production we find  $P_t \simeq -0.25$ ; for  $t\bar{b}$  production at LHC energies  $P_t \simeq -0.68$ , while  $P_t \simeq \mathcal{O}(-10^{-4})$  for  $t\bar{t}$  production. We have used the Madgraph+MadEvent [26] package to estimate these asymmetries for the SM processes. The very small value for the  $t\bar{t}$  mode is quite expected as the dominant contribution comes from the gluon induced process which does not have any axial component in the coupling. In Fig. 3 we plot the polarization asymmetry  $P_t$  given by Eq. (7) for both the

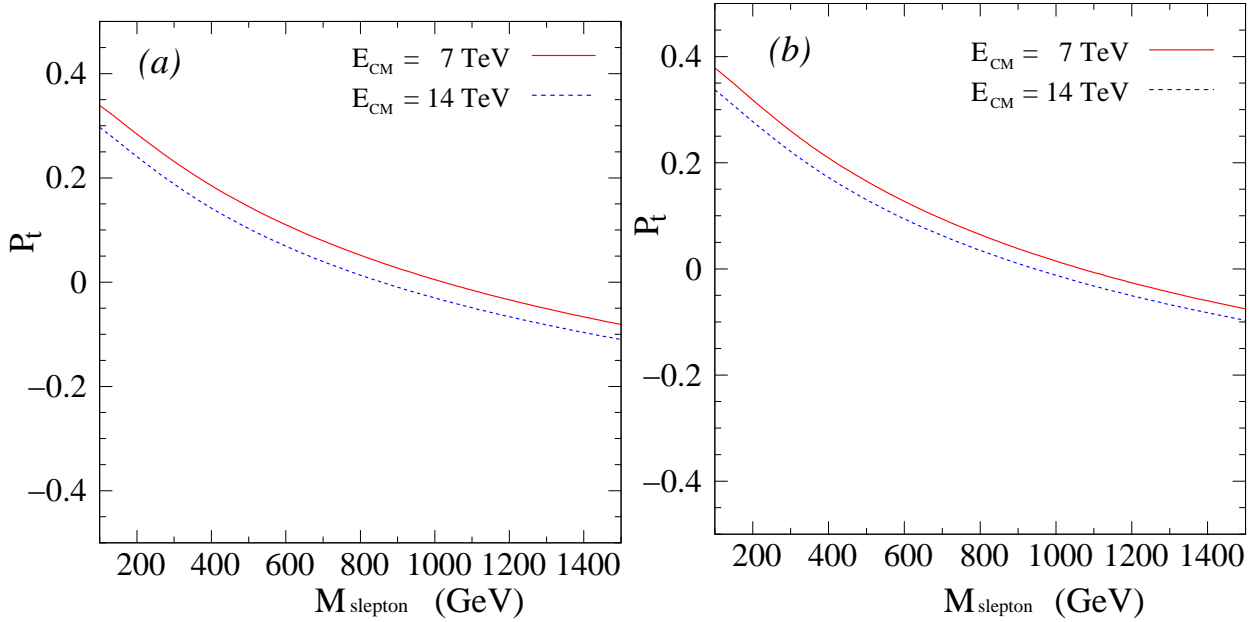


Figure 3: The polarization asymmetries for top-slepton production at LHC for two different center-of-mass energies, 7 TeV and 14 TeV. The asymmetry  $P_t$  is shown when the production is (a) via  $\lambda'_{i31}$  coupling and (b) via  $\lambda'_{i32}$  coupling.

$d$  and  $s$  quark induced processes. It is worth noting that at the tree-level,  $P_t$  is independent of the RPV coupling  $\lambda'_{i3k}$  which cancels out, but is still sensitive to the cross sections. So although the  $\lambda'_{i32}$  induced process shows slightly larger values for the asymmetry, it would be with limited statistics. However, the more interesting thing to note is that this asymmetry

is significantly different from what one expects in the SM processes and also of opposite sign (due to the  $P_R$  coupling), which forms the main thrust of this work. We see that for low values of the slepton mass, the polarization asymmetry can be as large as 0.33 and remains consistently positive for slepton masses  $\leq 850$  GeV. Another interesting feature is that the top polarization changes sign for a slepton mass of around 870-900 GeV. Thus a measurement of the sign of the longitudinal polarization asymmetry can prove to be a useful test for distinguishing top-slepton production from associated top production modes in the SM. Also, such a distinct value of the polarization asymmetry compared to the dominant mode of top quark production in the SM would imply that the asymmetry would leave an imprint in the distributions of the decay products as well as some distinct correlations in kinematic variables. This would also give an extra handle in suppressing the SM background.

### 3.2 The decays of the top quark and heavy slepton

In this section we discuss the decay of the top quark and the heavy slepton, needed to analyze the distinct final states, which we are interested in. As mentioned previously, the leptonic channel has the most sensitive analyzing power for the top quark polarization. The leptonic decay mode is further favored because of its cleanliness at the LHC. The respective branching ratios for top decays are well known, but we give the expressions for the top decay density matrix for completeness, which relates the decays to the  $2 \rightarrow 2$  production process via Eq. (5). The top decay density matrix for the process  $t \rightarrow bW^+ \rightarrow b\ell^+\nu_\ell$  can be written in a Lorentz invariant form as

$$\Gamma(\pm, \pm) = \frac{2g^4}{|p_W^2 - m_W^2 + i\Gamma_W m_W|^2} (p_b \cdot p_\nu) [(p_\ell \cdot p_t) \mp m_t(p_\ell \cdot n_3)], \quad (16)$$

for the diagonal elements and

$$\Gamma(\mp, \pm) = -\frac{2g^4}{|p_W^2 - m_W^2 + i\Gamma_W m_W|^2} m_t (p_b \cdot p_\nu) p_\ell \cdot (n_1 \mp i n_2), \quad (17)$$

for the off-diagonal ones. Here the  $n_i^\mu$ 's ( $i = 1, 2, 3$ ) are the spin 4-vectors for the top with 4-momentum  $p_t$ , with the properties  $n_i \cdot n_j = -\delta_{ij}$  and  $n_i \cdot p_t = 0$ . For decay in the rest frame they take the standard form  $n_i^\mu = (0, \delta_i^k)$ .

The slepton can decay through the R-parity conserving as well as R-parity violating

modes. The specific decays it can have are

$$\begin{aligned}\tilde{\ell}_{iL}^- &\rightarrow \ell_i^- \tilde{\chi}_j^0, \\ \tilde{\ell}_{iL}^- &\rightarrow \nu_{\ell_i} \tilde{\chi}_j^-, \\ \tilde{\ell}_{iL}^- &\rightarrow \bar{t} d_k \quad (\text{via RPV coupling}).\end{aligned}$$

Note that for the scalar slepton, the spin density matrix for its decay becomes trivial. The respective partial widths for each decay mode are given below:

$$\begin{aligned}\Gamma(\tilde{\ell}_{iL}^- \rightarrow \ell_i^- \tilde{\chi}_j^0) &= \frac{g^2 |(Z_{j2} + Z_{j1} \tan \theta_W)|^2}{32\pi} m_{\tilde{\ell}_{iL}} \left(1 - \frac{m_{\tilde{\chi}_j^0}^2}{m_{\tilde{\ell}_{iL}}^2} - \frac{m_{\ell_i}^2}{m_{\tilde{\ell}_{iL}}^2}\right) \lambda^{1/2} \left(1, \frac{m_{\tilde{\chi}_j^0}^2}{m_{\tilde{\ell}_{iL}}^2}, \frac{m_{\ell_i}^2}{m_{\tilde{\ell}_{iL}}^2}\right), \\ \Gamma(\tilde{\ell}_{iL}^- \rightarrow \nu_{\ell_i} \tilde{\chi}_j^-) &= \frac{g^2 |U_{ji}|^2}{16\pi} m_{\tilde{\ell}_{iL}} \left(1 - \frac{m_{\tilde{\chi}_j^-}^2}{m_{\tilde{\ell}_{iL}}^2}\right)^2, \\ \Gamma(\tilde{\ell}_{iL}^- \rightarrow \bar{t} d_k) &= 3 \frac{\lambda'_{i3k}}{16\pi} m_{\tilde{\ell}_{iL}} \left(1 - \frac{m_{d_k}^2}{m_{\tilde{\ell}_{iL}}^2} - \frac{m_t^2}{m_{\tilde{\ell}_{iL}}^2}\right) \lambda^{1/2} \left(1, \frac{m_{d_k}^2}{m_{\tilde{\ell}_{iL}}^2}, \frac{m_t^2}{m_{\tilde{\ell}_{iL}}^2}\right).\end{aligned}\tag{18}$$

The entries in the partial decay widths given by  $Z_{j2}, Z_{j1}$  correspond to the elements of the mixing matrix of the neutralinos, while  $U_{ji}$  represent the elements of the chargino mixing matrix. So, the respective branching ratios will depend on the SUSY parameters and the choice of RPV couplings. The lightest supersymmetric particle, which in our case is the neutralino is no longer stable in the RPV version of the model and will decay within the detector to SM particles via RPV couplings. The lightest neutralino has a 3-body decay [27] through the  $\lambda'_{i3k}$  couplings and being a Majorana fermion gives the decay products

$$\tilde{\chi}_1^0 \rightarrow \nu_i b \bar{d}_k, \quad \bar{\nu}_i \bar{b} d_k,\tag{19}$$

with equal probabilities. Note that we have assumed that the lightest neutralino is always lighter than the top quark and so its 3-body decay mode to a charged lepton-top quark and down quark ( $\ell_i t d_k$ ) is kinematically disallowed.

## 4 Signal Analysis

We now focus on the final states for our analysis and the dominant SM background contributing to such a final state. A quick glance at the decay modes suggest various possibilities to consider. As the slepton can decay to a lepton and a neutralino via R-parity conserving

mode, it would be the most desirable decay mode at LHC. To present our numerical results we assume a single non-zero RPV coupling given by  $\lambda'_{231}$  which fixes the initial quark  $d_k$  in the production process as the  $d$  quark. Also with this choice we consider only the smuon ( $\tilde{\mu}_L$ ) production in association with the top quark at LHC. We further assume that the charginos are much heavier than the sleptons and do not contribute in the decay of the smuon. We list below the possible combinations for the final states coming from the decay of the smuon and top quark.

- $t$  decays to 1  $b$ -jet and 2 light jets ( $J$ ) and  $\tilde{\mu}_L$  decays to a  $\mu^-$  and  $\tilde{\chi}_1^0$ .
  - $\mu^- + 2b\text{-jets} + 3J + \cancel{E}_T$ .
- $t$  decays to 1  $b$ -jet and 2 light jets and  $\tilde{\mu}_L$  decays to a  $\bar{t}$  and  $d$  quark.
  - $2b\text{-jets} + 5J$  ( $\bar{t}$  decays hadronically).
  - $\ell_j^- + 2b\text{-jets} + 2J + \cancel{E}_T$  ( $\bar{t}$  decays semileptonically).
- $t$  decays to 1  $b$ -jet,  $\ell_k^+$  and a neutrino while  $\tilde{\mu}_L$  decays to a  $\mu^-$  and  $\tilde{\chi}_1^0$ .
  - $\mu^- \ell_k^+ + 2b\text{-jets} + 1J + \cancel{E}_T$ .
- $t$  decays to 1  $b$ -jet,  $\ell_k^+$  and a neutrino while  $\tilde{\mu}_L$  decays to a  $\bar{t}$  and  $d$  quark.
  - $\ell_k^+ + 2b\text{-jets} + 3J + \cancel{E}_T$  ( $\bar{t}$  decays hadronically).
  - $\ell_j^- \ell_k^+ + 2b\text{-jets} + 1J + \cancel{E}_T$  ( $\bar{t}$  decays semileptonically).

As pointed out earlier in Section 2, the effects of top polarization are more sensitive through the lepton in its semileptonic decay mode. In addition we hope to understand the leptonic signal at the LHC with much better precision compared to signals with large hadronic activity. Also extra efforts are in place to study the  $b$ -jets at LHC with greater efficiency. Keeping this in mind, we focus on triggering upon the dilepton final state with two  $b$ -jets and large missing transverse momenta with no light quark jets. We do not consider triggering on a light jet in the signal, since the light jet comes from the 3-body decay of the neutralino and is expected to be soft. Such a soft jet will not help against the SM background as one naturally expects a lot of associated soft jet multiplicity at LHC due to radiation. We

also consider the two leptons to be of different flavor which makes the signal more distinct and robust. So the signal in question would be

$$pp \longrightarrow \mu^- e^+ b \bar{b} + \cancel{E}_T + X. \quad (20)$$

The most dominant SM background would come from the  $t\bar{t}$  production as well as triple gauge boson (TGB) production ( $WWZ$ ) where the  $Z$  decays to  $b\bar{b}$ . The TGB background can be brought under control by a cut on the invariant mass of  $b\bar{b}$ . So we mainly focus on the  $t\bar{t}$  background. It is also of interest to consider the  $tW$  background as we would like to focus on the effect of top polarization on the signal and compare it with the dominant SM sources for a similar final state given in Eq. (20). For our analysis we choose two different representative points in the SUSY parameter space given in Table 1. We list only the relevant inputs and the masses needed for our analysis. They represent a light and heavy smuon which will highlight, how the different kinematics help in distinguishing the signal from the background as well as the effects of top polarization on the distributions. To calculate and generate

Parameters	I	II
$(M_1, M_2)$	(100, 300)	(100, 500)
$A_i$	-1000	-1500
$(\mu, \tan \beta)$	(250, 10)	(600, 5)
$(M_{\ell L}, M_{\ell R})$	(200, 200)	(500, 500)
$(M_{\tilde{\chi}_1^0}, M_{\tilde{\chi}_1^\pm})$	(93, 218)	(97, 478)
$(m_{\tilde{\ell}_L}, m_{\tilde{\ell}_R})$	(205, 205)	(502, 502)
$m_{\tilde{\nu}L}$	190	496
$\lambda'_{231}$	0.2	0.5

Table 1: *Representative points in the MSSM parameter space and the relevant mass spectrum used in the analysis. All mass parameters are given in units of GeV. To generate the mass spectrum for the supersymmetric particles we have used the code Suspect [28].*

events for the final state given by Eq. (20) and study the effects of top polarization on the kinematics, we are required to keep the spin information of the top quark in its production and decay. For this purpose we have used the package *Madgraph+MadEvent* [26] with its explicit use of helicity amplitudes. We have included the relevant vertices for the RPV

interactions and used this package to calculate the signal as well as the SM background, namely the final states coming from the  $t\bar{t}$  and  $tW$  production. We must point out here that the  $tW$  background is only considered for the purpose of comparing the distributions of the top decay products to highlight the polarization effect due to different interaction vertices involved in its production.

For triggering on the final states, we set the following kinematic cuts

- The charged leptons must have a minimum  $p_T$  of 10 GeV and lie within the rapidity gap given by  $|\eta^\ell| < 2.5$ .
- The  $b$ -jets in the final state must satisfy  $p_T > 20$  GeV and respect the rapidity cut of  $|\eta^b| < 2.5$ .
- The final states must account for a minimum missing transverse energy,  $\cancel{E}_T > 50$  GeV.
- To ensure proper spatial resolution between the final state particles we demand that  $\Delta R_{\ell_i \ell_j} > 0.2$ ,  $\Delta R_{\ell b} > 0.4$  and  $\Delta R_{bb} > 0.7$  where  $\ell$  represents the charged leptons. The  $\Delta R$  between two particles is defined as  $\Delta R_{AB} = \sqrt{\Delta\phi_{AB}^2 + \Delta\eta_{AB}^2}$ , with  $\Delta\phi$  and  $\Delta\eta$  being the separation in the azimuthal angle and the rapidity of the two particles.

With this set of kinematic cuts we calculate the signal for the two representative points given in Table 1. We have assumed a  $b$ -jet identification efficiency of 50%. We must point out here that for our parton-level analysis, the  $b$ -jet is represented by the parent  $b$ -quark produced in the final state. Since the signal is sensitive to the strength of the RPV coupling, whose limits are dependent on the squark masses, we use conservative values for the couplings by setting the squark masses to 1 TeV. For our choice of the RPV couplings listed in Table 1, we find that the signal satisfying the above set of kinematic cuts at LHC with the initial run of  $\sqrt{s} = 7$  TeV, is 4.3 fb for  $m_{\tilde{\mu}_L} = 205$  GeV, while it is 8.4 fb for  $m_{\tilde{\mu}_L} = 502$  GeV. The main decay modes that contribute to the signal depend on the respective branching ratios. The branching ratios for the two cases are given by

$$\begin{aligned} BR(\tilde{\mu}_L \rightarrow \mu \tilde{\chi}_1^0) &= 0.76, \quad BR(\tilde{\mu}_L \rightarrow \bar{t}d) = 0.24 \quad (m_{\tilde{\mu}_L} = 205 \text{ GeV}), \\ BR(\tilde{\mu}_L \rightarrow \mu \tilde{\chi}_1^0) &= 0.09, \quad BR(\tilde{\mu}_L \rightarrow \bar{t}d) = 0.90 \quad (m_{\tilde{\mu}_L} = 502 \text{ GeV}). \end{aligned}$$

For the lighter smuon, the signal is completely dominated by the contributions coming from the R-parity conserving decay of smuon. Although the RPV decay is around 24%, the small

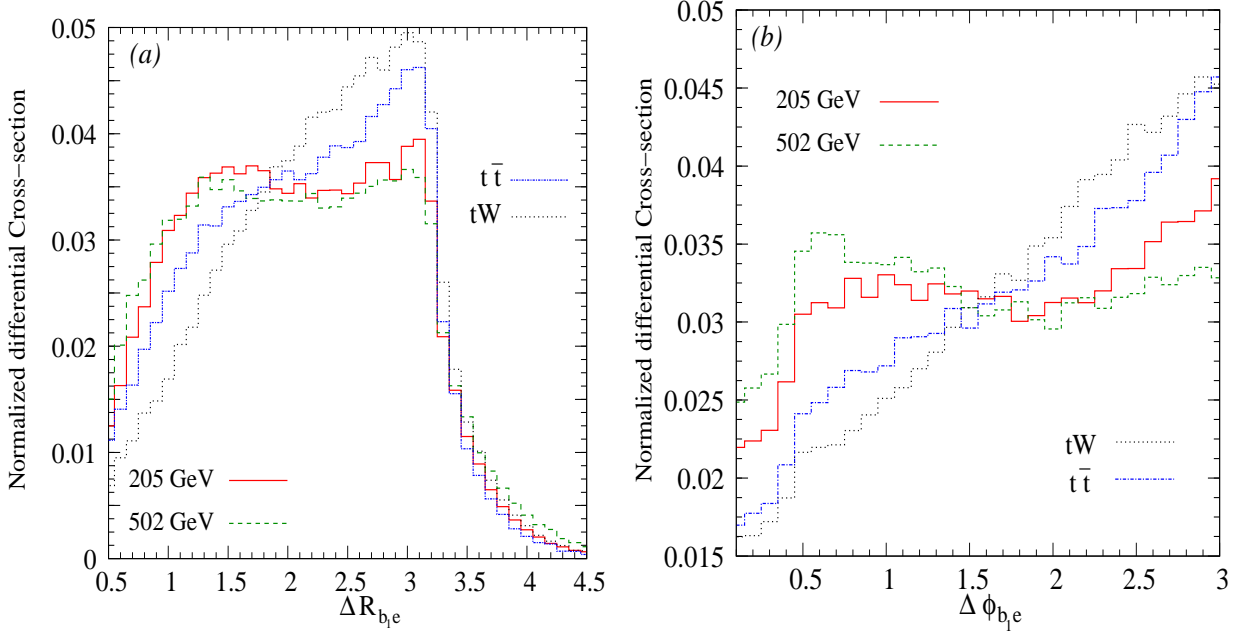


Figure 4: Showing the normalized distributions for the signal with two different smuon mass of 205 GeV and 502 GeV as well as the competing SM background for associated top quark production. In (a) we show the separation in  $\Delta R_{b_1e}$  while in (b) we show the azimuthal separation  $\Delta\phi_{b_1e}$ . Here both  $e$  and  $b_1$  which represents the leading  $b$ -jet, primarily come from the top quark decay.

branching fraction for the top quark decay to the leptonic mode makes its contribution very small. However, for the heavier smuon the RPV decay is 90% and hence contributes significantly to the final states. In fact we find that it contributes to about 58% of the signal. For the 14 TeV collisions at LHC with the same kinematic cuts on the events, there is a significant increase in the signal, which is around 13.2 fb for  $m_{\tilde{\mu}_L} = 205$  GeV while it is 48 fb for  $m_{\tilde{\mu}_L} = 502$  GeV. In comparison to the signals, we find that the SM background for the same kinematic selection cuts, is very large with the  $t\bar{t}$  contributions at leading order (LO) coming out to be  $\sim 145$  fb for the 7 TeV machine while it is  $\sim 780$  fb for the 14 TeV collisions. The K-factors for both the signal and background will help in reducing the uncertainties in the statistics. However even with the LO results of the signal, one can see that with a high luminosity of  $100 \text{ fb}^{-1}$ , the signal can be significant.

It is also worth noting that as the muon in the final state comes from a heavy smuon, it will have a larger  $p_T$  compared to the muon which comes from the decays of  $W$  boson in



the SM. So a stronger  $p_T$  cut for the muon in the final state will also help in reducing the SM background [7]. As an estimate we put a stronger cut on the muon by choosing  $p_T^\mu > 40$  GeV at the  $\sqrt{s} = 7$  TeV collisions. The signal becomes 3.2 fb and 6.4 fb for the light and heavy smuon, respectively. But there is a much stronger suppression for the SM background coming from  $t\bar{t}$ , which becomes 80 fb at the LO. This increases the significance of the signal a lot. In fact a much stronger  $p_T$  cut on the muon is desirable for the heavy smuon signal which would be very effective in reducing the large SM background [7]. We discuss more on the effects of various kinematic cuts on the signal and background at the LHC in Section 5.

Let us now try and see what effect the strong polarization asymmetry (Fig. 3) for the associated top production at LHC via the chirality violating coupling  $\lambda'_{231}$  has on the final states. In Fig. 4 we show the distribution of particles which come directly from the decay of the top quark. In Fig. 4 (a) we plot the spatial separation ( $\Delta R$ ) in the  $(\eta, \phi)$  plane between the leading  $b$ -jet ( $b_1$ ) and the electron, coming primarily from the top quark decay, for the signal and the SM background. The normalized distributions show that there is a significant difference in the distributions for the decay products of the top quark for the signal when compared with the SM subprocesses. The difference is much better highlighted in the  $\Delta\phi$  distribution as shown in Fig. 4 (b). This shows that a  $\Delta\phi$  difference is a clear highlight of the top polarization effect on the distributions. Although it does not give a direct estimate of the polarization of the top quark, it gives a very clear indication of its importance as a probe to study the effect of a chirality violating coupling responsible for its production when compared to SM. We find that the above distributions do not change much for muon  $p_T$  cuts of less than 40-50 GeV. However much stronger  $p_T$  cuts on the muon result in events with highly boosted tops which significantly affect the angular correlation.

In Fig. 5 we show a few kinematic distributions, which are sensitive to the muon energy as well as to the nature of the mother particle it comes from. In Fig. 5(a) we plot the normalized cross section with respect to the ratio between the energy of the muon and the sum of the energy of the muon and the sub-leading  $b$ -jet,  $E_\mu/(E_{b_2} + E_\mu)$ . This is a variable which directly reflects the energy strength of the muon in the smuon decay chain. As the sub-leading  $b$ -jet dominantly comes from the 3-body decay of the neutralino, this ratio will always peak for values greater than 0.5 as the muon comes from the primary decay of smuon and carries energy depending on the mass difference between the smuon and neutralino. The SM background contribution to this ratio is peaked for values less than 0.5 since the muon

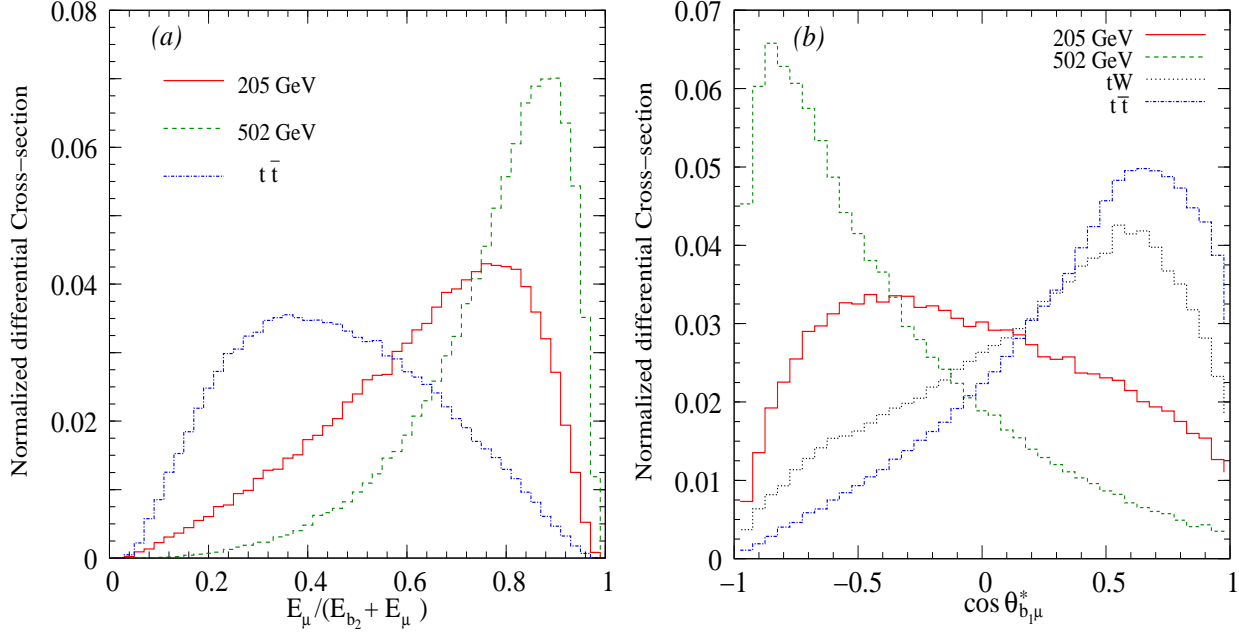


Figure 5: Showing the normalized distributions for the signal with two different smuon mass of 205 GeV and 502 GeV as well as the competing SM background for associated top quark production. In (a) we show the relative strength of the energy of  $\mu$  and in (b) we show the angular variation of the  $\mu$  in a special frame (explained in text).

in this case comes from the decay of the  $W$  boson, while the sub-leading  $b$ -jet always comes from the top decay. The ratio, however, does depend on the relative mass differences as is evident from Fig. 5 (a) which shows the sharp shift in the value for the heavier smuon as compared to the lighter smuon. The ratio will also be sensitive to the  $p_T$  cuts. Nevertheless, it is an effective variable to distinguish the signal from the SM background.

Fig. 5 (b) shows an even more interesting distribution. It is the cosine of the angle constructed in the rest frame of the muon and the leading  $b$ -jet and represents the angle between the direction of the muon in this frame with respect to the boost direction of the muon plus  $b$ -jet system. We find that this variable is quite sensitive to the nature of the mother particle of the muon. As shown in the figure, both for the  $t\bar{t}$  and the  $tW$  backgrounds the muon, which always comes from the decay of the  $W$  boson, is peaked for  $\cos \theta_{b_1 \mu}^* > 0$  while it peaks for  $\cos \theta_{b_1 \mu}^* < 0$  for the case when it comes from the decay of the scalar particle ( $\tilde{\mu}_L$ ). This gives a very clear hint of the different nature of the spin of the particle, if not the spin itself. It will be interesting to see if this variable can help to distinguish between

signals of universal extra dimensions model, which is often called the "bosonic" SUSY. One could also consider various asymmetries in the above variables, which can also prove to be useful tools in distinguishing the signal from the SM background.

We have till now focused only on the R-parity conserving decays of the smuon to highlight the signal. However, the muon can also come from the semileptonic decay of the top quark, if the RPV decay dominates as is the case for  $m_{\tilde{\mu}_L} = 502$  GeV. We now focus on how

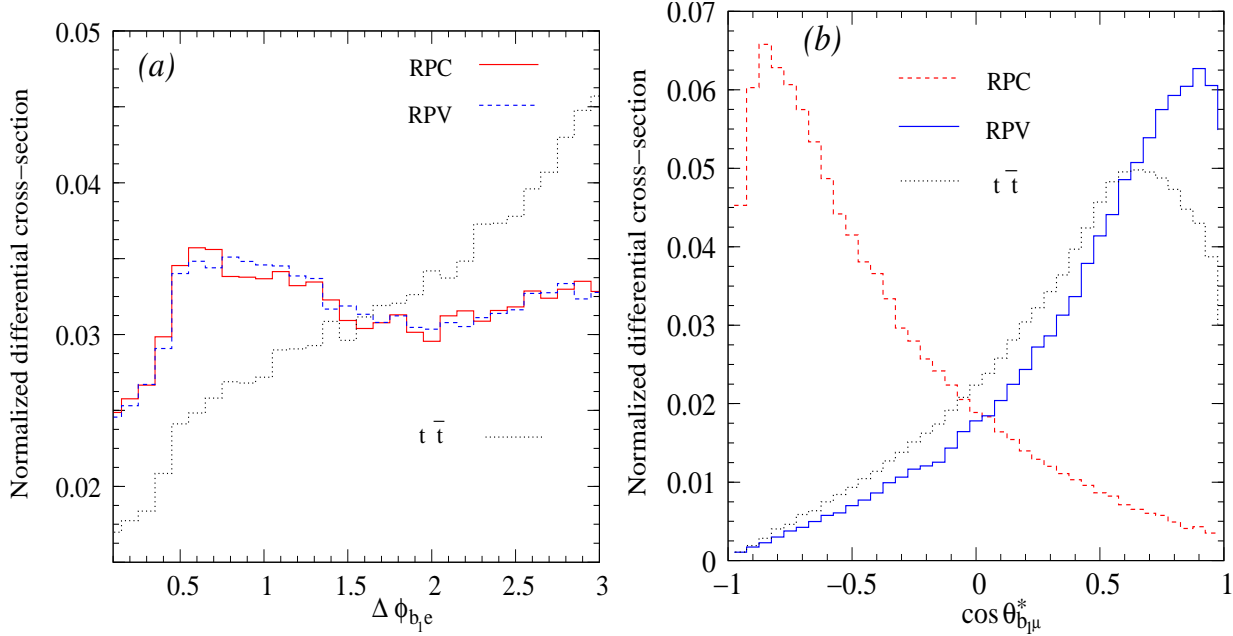


Figure 6: Showing the normalized distributions of the signal for the R-parity conserving (RPC) and R-parity violating (RPV) decays of the smuon of mass 502 GeV as well as the SM background from  $t\bar{t}$ . In (a) we show the azimuthal separation  $\Delta\phi_{b1e}$  (Fig. 4 (b)). In (b) we show the angular variation of the  $\mu$  (Fig. 5 (b)).

this may affect the distributions. As already stated before, the distributions shown in Fig. 4 represent the decay products of the top quark and are, therefore, not affected as long as the top quark is produced in association with the slepton. To show this, we plot the normalized distributions again for  $m_{\tilde{\mu}_L} = 502$  GeV in Fig. 6 (a) where we consider both the R-parity conserving decay given by  $\tilde{\mu}_L^- \rightarrow \mu^- \tilde{\chi}_1^0$  and the RPV decay  $\tilde{\mu}_L^- \rightarrow \bar{t} d$  separately. Note that the muon ( $\mu^-$ ) now comes from the decay of  $\bar{t}$  and should therefore also highlight the polarization of the antitop. We show that the  $\Delta\phi_{b1e}$  distribution remains unaffected and also the normalized  $\Delta\phi_{b1\mu}$  distribution is found to overlap with the  $\Delta\phi_{b1e}$  distribution.

cut-1	$p_T^\mu > 10 \text{ GeV}, p_T^e > 10 \text{ GeV}, p_T^b > 20 \text{ GeV}, \cancel{E}_T > 50 \text{ GeV},$ $ \eta^{\ell,b}  < 2.5, \Delta R_{e\mu} > 0.2, \Delta R_{\ell b} > 0.4, \Delta R_{bb} > 0.7$
cut-2a	$p_T^\mu > 60 \text{ GeV}, p_T^e > 10 \text{ GeV}, p_T^b > 20 \text{ GeV}, \cancel{E}_T > 50 \text{ GeV},$ $ \eta^{\ell,b}  < 2.5, \Delta R_{e\mu} > 0.2, \Delta R_{\ell b} > 0.4, \Delta R_{bb} > 0.7$
cut-2b	$p_T^\mu > 100 \text{ GeV}, p_T^e > 10 \text{ GeV}, p_T^b > 20 \text{ GeV}, \cancel{E}_T > 50 \text{ GeV},$ $ \eta^{\ell,b}  < 2.5, \Delta R_{e\mu} > 0.2, \Delta R_{\ell b} > 0.4, \Delta R_{bb} > 0.7$
cut-3	$p_T^\mu > 10 \text{ GeV}, p_T^e > 10 \text{ GeV}, p_T^b > 20 \text{ GeV}, \cancel{E}_T > 50 \text{ GeV},$ $ \eta^{\ell,b}  < 2.5, \Delta R_{e\mu} > 0.2, \Delta R_{\ell b} > 0.4, \Delta R_{bb} > 0.7, \Delta\phi_{b_1e} < 1.5$
cut-4a	$p_T^\mu > 60 \text{ GeV}, p_T^e > 10 \text{ GeV}, p_T^b > 20 \text{ GeV}, \cancel{E}_T > 50 \text{ GeV},$ $ \eta^{\ell,b}  < 2.5, \Delta R_{e\mu} > 0.2, \Delta R_{\ell b} > 0.4, \Delta R_{bb} > 0.7, \Delta\phi_{b_1e} < 1.5$
cut-4b	$p_T^\mu > 100 \text{ GeV}, p_T^e > 10 \text{ GeV}, p_T^b > 20 \text{ GeV}, \cancel{E}_T > 50 \text{ GeV},$ $ \eta^{\ell,b}  < 2.5, \Delta R_{e\mu} > 0.2, \Delta R_{\ell b} > 0.4, \Delta R_{bb} > 0.7, \Delta\phi_{b_1e} < 1.5$

Table 2: *Different choices for kinematic cuts on the final states  $\mu^-e^+b\bar{b} + \cancel{E}_T + X$  to study the LHC reach.*

Thus both the muon as well as the electron carry the information of the chirality violating vertex of the  $t$  and  $\bar{t}$  with the  $\tilde{\mu}_L$ . The other plot (Fig. 5 (b)) which represents the spin information of the mother particle should however change since the muon now comes from the semileptonic decay of the anti-top quark and should be similar to the  $t\bar{t}$  contribution. This, in fact turns out to be same when considered separately as shown in Fig. 6(b). This clearly shows that the angular distribution shown is directly sensitive to the nature of the mother particle it originates from.

## 5 Signal potential at the LHC

In this section we discuss the signal potential for the single slepton production at the LHC. As the dominant background comes from the  $t\bar{t}$  production, we would like to see which cuts would be relevant for suppressing the background without affecting much of the signal cross section. The most important kinematic variable turns out to be the muon transverse momentum. The muon coming from the primary decay of the smuon has a large  $p_T$  as compared to the muon coming from the semileptonic decay of the top quark. Also most of

Cuts	$\sqrt{s} = 7 \text{ TeV}$			$\sqrt{s} = 14 \text{ TeV}$		
	$m = 205 \text{ GeV}$	$m = 502 \text{ GeV}$	SM	$m = 205 \text{ GeV}$	$m = 502 \text{ GeV}$	SM
<i>cut-1</i>	17.2	33.6	579.3	52.8	192.3	3127.5
<i>cut-2a</i>	9.8	19.8	182.2	35.5	111.7	1026.7
<i>cut-2b</i>	–	–	–	17.5	84.7	334.2
<i>cut-3</i>	6.8	16.1	218.6	24.5	93.9	1192.0
<i>cut-4a</i>	4.6	9.5	79.6	17.5	55.2	455.1
<i>cut-4b</i>	–	–	–	9.6	42.5	177.6

Table 3: *The leading order cross sections (in fb) for the kinematic cuts listed in Table 2 on the final states  $\mu^- e^+ b\bar{b} + \cancel{E}_T + X$  for the signal and the SM background. No efficiency factors included for the  $b$ -jets in this table.*

the kinematic variables described in the previous section depend on our cut on the muon  $p_T$ . So our choice of the transverse momenta cut on the muon also becomes quite relevant for studying the top polarization effects, since the angular correlations (in the decay products) are likely to get washed away for very boosted top quarks.

In Table 2, we list different set of kinematic cuts with changes in the cuts for the muon  $p_T$  and the  $\Delta\phi_{b_1e}$  variable and show at what significance the signal can be observed at LHC. The *cut-1* corresponds to the minimal set where we have the distinct correlation in the azimuthal angular distributions highlighting the top polarization effects as shown in Fig. 4. The *cut-2a* and *cut-2b* represent strong  $p_T$  cuts on the muon of 60 GeV and 100 GeV respectively, while *cut-3* corresponds to a  $\Delta\phi_{b_1e} < 1.5$  cut (to exploit the large asymmetry seen for SM in Fig. 4(b) for *cut-1*) to reduce the SM background. The cuts defined by *cut-4a* and *cut-4b* again represent strong  $p_T$  cuts on the muon of 60 GeV and 100 GeV respectively, with the additional cut of  $\Delta\phi_{b_1e} < 1.5$ .

In Table 3 we give the total cross section for the final states  $\mu^- e^+ b\bar{b} + \cancel{E}_T + X$  for the signal for two values of the smuon mass and also the SM background at LHC with the different kinematic cuts listed in Table 2. We can see that the strong cuts on the  $p_T$  of muon turn out to be most effective in improving the significance of the signal. We have not included any  $b$ -tagging efficiency factors for the cross sections given in Table 3. Including a  $b$ -tagging efficiency of 50% one can find that for the case of smuon of mass 205 GeV and with

$\sqrt{s} = 7$  (14) TeV center-of-mass energy at LHC, one can get a significance  $S = 3.63$  (5.54) with *cut-2a* for a luminosity of  $100 \text{ fb}^{-1}$ . It is however worth noting that with *cut-1* one still has appreciable signal significance ( $S = 3.57$  (4.72)) for the lighter smuon. We have defined the *significance* as  $S = \frac{N_s}{\sqrt{N_{SM}}}$ , where  $N_s$  represents the number of events coming from the RPV contribution and  $N_{SM}$  is the number of events for the SM background. We have excluded the values for the cross sections for the 7 TeV run at LHC for the more stronger cuts given by *cut-2b* and *cut-4b* in Table 3 which also have strong suppressions for the signal.

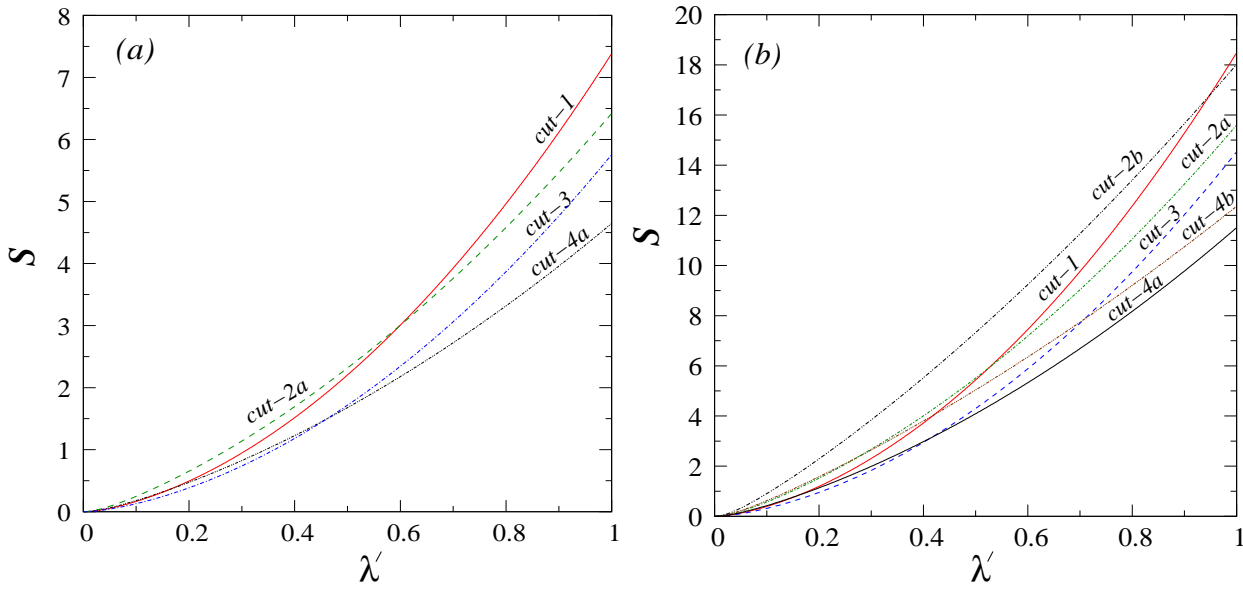


Figure 7: The significance ( $S$ ) is shown for the different kinematic cuts, as a function of RPV coupling ( $\lambda'$ ) for a fixed integrated luminosity ( $L = 10 \text{ fb}^{-1}$ ) and smuon mass ( $m_{\tilde{\mu}_L} = 502 \text{ GeV}$ ) for two different center-of-mass energies, (a)  $\sqrt{s} = 7 \text{ TeV}$  and (b)  $\sqrt{s} = 14 \text{ TeV}$ .

In Fig. 7 we plot the significance as a function of the RPV coupling  $\lambda'$  for the smuon of mass,  $m_{\tilde{\mu}_L} = 502 \text{ GeV}$ . It is important to note here that both the production cross section for the single top production with the smuon and the decay properties of the smuon depend on the value of  $\lambda'$ . For small values of  $\lambda'$  the R-parity conserving decay of the smuon ( $\tilde{\mu}_L^- \rightarrow \mu^- \tilde{\chi}_1^0$ ) is the primary source for the signal. However, as the RPV coupling becomes larger, the RPV decay mode of the smuon ( $\tilde{\mu}_L^- \rightarrow \bar{t}d$ ) becomes the dominant source for the signal and the muon then mostly comes from the semileptonic decay of the anti-top. This would mean that a strong  $p_T$  cut on the muon also causes suppression of the signal for large

$\lambda'$  coupling. This is illustrated in Fig. 7 where we have chosen the integrated luminosity as  $10 \text{ fb}^{-1}$ . We find that the significance for the strong cut on the muon  $p_T > 100 \text{ GeV}$  (*cut-2b*) becomes comparable to *cut-1* for larger values of  $\lambda'$  as compared to smaller values of  $\lambda'$ . It is also found that the cut on the variable  $\Delta\phi_{b_1e}$  (*cut-3*) also gives a reasonably high significance, but is not as effective as the cut on the muon  $p_T$ .

## 6 Summary

We have studied the single production of a slepton in association with a top quark at the LHC. Our analysis has focused on describing the effects of the top polarization on the particular signal of an associated charged slepton and we have shown that the Lorentz structure at the production vertex for the top can lead to very distinct signals, which have not been considered in the literature. We find that the polarization asymmetry is significantly different from the SM expectation for a very wide range of slepton mass accessible at the LHC. However, the work relies on violating R-parity in SUSY so that we can produce a single slepton. A natural extension to this work would be to look at the associated production of top with charged Higgs [29, 30] which would be challenging as the leptonic mode (first 2 generations) of decay is suppressed. However, as seen in Fig. 6 (a), the top polarization effects would still show up in some kinematic distributions. Another interesting variable that we have found through our analysis is the  $\cos\theta^*$  variable for a final state particle. It is found to be sensitive to the spin of the mother particle it originates from. It would be interesting to study this variable in order to distinguish models, which predict particles with different spins.

In our numerical analysis we have chosen only one non-zero  $\lambda'$  coupling. This study can also be replicated for other  $\lambda'$  couplings, leading to different final states. However, the interesting kinematic features studied and highlighted for the final states would still hold and can prove to be useful tools in constraining the RPV couplings.

### Acknowledgments:

S.K.R. would like to thank A. Khanov and F. Rizatdinova for useful discussions. This work was supported in part by the Research Program MSM6840770029 and by the project of International Cooperation ATLAS-CERN of the Ministry of Education, Youth and Sports of the Czech Republic (M. A.). K.H. and K.R. gratefully acknowledge the support from

the Academy of Finland (Project No. 115032). S.K.R. is supported by US Department of Energy, Grant Number DE-FG02-04ER41306.

## References

- [1] P. Fayet, Phys. Lett. B **69**, 489 (1977); G. R. Farrar and P. Fayet, Phys. Lett. B **76**, 575 (1978).
- [2] A. Y. Smirnov and F. Vissani, Phys. Lett. B **380** (1996) 317 [arXiv:hep-ph/9601387]; Nucl. Phys. B **460** (1996) 37 [arXiv:hep-ph/9506416].
- [3] L. E. Ibanez and G. G. Ross, Phys. Lett. B **260**, 291 (1991); L. E. Ibanez and G. G. Ross, Nucl. Phys. B **368**, 3 (1992).
- [4] L. J. Hall and M. Suzuki, Nucl. Phys. B **231** (1984) 419.
- [5] R. Barbier *et al.*, Phys. Rept. **420**, 1 (2005).
- [6] For a summary of these limits, see for example,  
G. Bhattacharyya, hep-ph/9709395; B.C. Allanach, A. Dedes and H.K. Dreiner, Phys. Rev. **D60** 075014,1999; M. Chemtob, Prog. Part. Nucl. Phys. **54** 71 (2005).
- [7] M. A. Bernhardt, H. K. Dreiner, S. Grab and P. Richardson, Phys. Rev. D **78** (2008) 015016 [arXiv:0802.1482 [hep-ph]].
- [8] A. Datta, J. M. Yang, B. L. Young and X. Zhang, Phys. Rev. D **56** (1997) 3107 [arXiv:hep-ph/9704257]; R. J. Oakes, K. Whisnant, J. M. Yang, B. L. Young and X. Zhang, Phys. Rev. D **57** (1998) 534 [arXiv:hep-ph/9707477]; P. Chiappetta, A. Deandrea, E. Nagy, S. Negroni, G. Polesello and J. M. Virey, Phys. Rev. D **61** (2000) 115008 [arXiv:hep-ph/9910483]; F. Borzumati, J. L. Kneur and N. Polonsky, Phys. Rev. D **60** (1999) 115011 [arXiv:hep-ph/9905443]; Z. H. Yu, P. Herbert, W. G. Ma, L. Han and Y. Jiang, arXiv:hep-ph/9910323; M. Chaichian, K. Huitu and Z. H. Yu, Phys. Lett. B **490** (2000) 87 [arXiv:hep-ph/0007220]; T. M. P. Tait and C. P. P. Yuan, Phys. Rev. D **63** (2001) 014018 [arXiv:hep-ph/0007298]; Z. Hong, M. Wen-Gan, J. Yi, Z. Ren-You and W. Lang-Hui, Phys. Rev. D **64** (2001) 095006; J. Cao, Z. Heng, L. Wu and J. M. Yang, Phys. Rev. D **79** (2009) 054003 [arXiv:0812.1698 [hep-ph]].



- [9] D. O. Carlson and C. P. Yuan, Phys. Lett. B **306** (1993) 386; A. Heinson, A. S. Belyaev and E. E. Boos, Phys. Rev. D **56** (1997) 3114 [arXiv:hep-ph/9612424]; T. Stelzer, Z. Sullivan and S. Willenbrock, Phys. Rev. D **58** (1998) 094021 [arXiv:hep-ph/9807340]; E. E. Boos and A. V. Sherstnev, Phys. Lett. B **534** (2002) 97 [arXiv:hep-ph/0201271].
- [10] G. Mahlon and S. J. Parke, Phys. Rev. D **55** (1997) 7249 [arXiv:hep-ph/9611367]; G. Mahlon and S. J. Parke, Phys. Lett. B **476** (2000) 323 [arXiv:hep-ph/9912458].
- [11] M. Chemtob and G. Moreau, Phys. Rev. D **61** (2000) 116004 [arXiv:hep-ph/9910543].
- [12] K. i. Hikasa, J. M. Yang and B. L. Young, Phys. Rev. D **60** (1999) 114041 [arXiv:hep-ph/9908231].
- [13] P. Y. Li, G. R. Lu, J. M. Yang and H. Zhang, Eur. Phys. J. C **51**, 163 (2007) [arXiv:hep-ph/0608223].
- [14] M. Arai, N. Okada, K. Smolek and V. Simak, Phys. Rev. D **70** (2004) 115015 [arXiv:hep-ph/0409273]; Phys. Rev. D **75** (2007) 095008 [arXiv:hep-ph/0701155]; Acta Phys. Polon. B **40** (2009) 93 [arXiv:0804.3740 [hep-ph]]; M. Arai, N. Okada and K. Smolek, Phys. Rev. D **79** (2009) 074019 [arXiv:0902.0418 [hep-ph]].
- [15] R. M. Godbole, S. D. Rindani and R. K. Singh, JHEP **12**, 021 (2006); R. M. Godbole, S. D. Rindani, K. Rao and R. K. Singh, AIP Conf. Proc. **1200** (2010) 682 [arXiv:0911.3622 [hep-ph]].
- [16] [Tevatron Electroweak Working Group and CDF Collaboration and D0 Collab], arXiv:0903.2503 [hep-ex].
- [17] I. I. Y. Bigi, Y. L. Dokshitzer, V. A. Khoze, J. H. Kuhn and P. M. Zerwas, Phys. Lett. B **181**, 157 (1986).
- [18] W. Bernreuther, J. Phys. G: Nucl. Part. Phys. **35**, 083001 (2008).
- [19] M. Beneke *et al.*, arXiv:hep-ph/0003033.
- [20] W. Wagner, Rept. Prog. Phys. **68**, 2429 (2005).

- [21] M. Jezabek and J. H. Kuhn, Phys. Lett. B **329**, 317 (1994) [arXiv:hep-ph/9403366].
- [22] A. Czarnecki, M. Jezabek and J. H. Kuhn, Nucl. Phys. B **351** (1991) 70.
- [23] W. Bernreuther, O. Nachtmann, P. Overmann and T. Schroder, Nucl. Phys. B **388**, 53 (1992) [Erratum-ibid. B **406**, 516 (1993)].
- [24] J. P. Ma and A. Brandenburg, Z. Phys. C **56**, 97 (1992).
- [25] J. Pumplin, A. Belyaev, J. Huston, D. Stump and W. K. Tung, JHEP **0602**, 032 (2006) [arXiv:hep-ph/0512167].
- [26] T. Stelzer and W. F. Long, Comput. Phys. Commun. **81**, 357 (1994) [arXiv:hep-ph/9401258]; F. Maltoni and T. Stelzer, JHEP **0302**, 027 (2003) [arXiv:hep-ph/0208156].
- [27] E. A. Baltz and P. Gondolo, Phys. Rev. D **57**, 2969 (1998) [arXiv:hep-ph/9709445].
- [28] A. Djouadi, J. L. Kneur and G. Moultaka, Comput. Phys. Commun. **176**, 426 (2007) [arXiv:hep-ph/0211331].
- [29] M. Beccaria, F. M. Renard and C. Verzegnassi, Phys. Rev. D **71**, 033005 (2005); M. Beccaria, G. Macorini, L. Panizzi, F. M. Renard and C. Verzegnassi, Phys. Rev. D **80**, 053011 (2009) [arXiv:0908.1332 [hep-ph]].
- [30] K. Huitu *et al.*, *Work in progress*.